Power-law behavior of transcriptional bursting regulated by enhancer-promoter communication

Zihao Wang, Zhenquan Zhang, Songhao Luo, et al.

Genome Res. published online January 3, 2024
Access the most recent version at doi:10.1101/gr.278631.123

Power-law behavior of transcriptional bursting regulated by enhancer-promoter communication

Zihao Wang[a,b,1], Zhenquan Zhang[a,b,1], Songhao Luo[a,b,1], Tianshou Zhou[a,b,2], and Jiajun Zhang[a,b,2]

[a] Guangdong Province Key Laboratory of Computational Science, Sun Yat-sen University, Guangzhou 510275, P. R. China

[b] School of Mathematics, Sun Yat-sen University, Guangzhou 510275, P. R. China

[1] These authors contributed equally to this work.

[2] To whom correspondence may be addressed.

Email: mcszhtsh@mail.sysu.edu.cn or zhjiajun@mail.sysu.edu.cn

Abstract

Revealing how transcriptional bursting kinetics is genomically encoded is challenging since genome structures are stochastic at the organization level and are suggestively linked to gene transcription. To address this challenge, we develop a generic theoretical framework that integrates chromatin dynamics, enhancer-promoter (E-P) communication and gene-state switching, to study transcriptional bursting. The theory predicts that power law can be a general rule to quantitatively describe bursting modulations by E-P spatial communication. Specifically, burst frequency and burst size are up-regulated by E-P communication strength, following power laws with positive exponents. Analysis of the scaling exponents further reveals that burst frequency is preferentially regulated. Bursting kinetics are down-regulated by E-P genomic distance with negative power-law exponents, and this negative modulation desensitizes at large distances. The mutual information between burst frequency (or burst size) and E-P spatial distance further reveals essential characteristics of the information transfer from E-P communication to transcriptional bursting kinetics. These findings, which are in agreement with experimental observations, not only reveal fundamental principles of E-P communication in transcriptional bursting but also are essential for understanding cellular decision-making.

Introduction

Gene transcription that is tightly related to three-dimensional (3D) genomic organization is a highly complex and regulated process that exhibits a discontinuous episodic bursting behavior (Misteli, 2020; Rodriguez and Larson, 2020; Suter et al., 2011; Tunnacliffe and Chubb, 2020). As two cardinal regulatory elements, the promoter and the enhancer are responsible for the accurate spatiotemporal gene expression ensuring reliable cell functioning and cellular decision-making (Robson et al., 2019; Stadhouders et al., 2019; Zabidi and Stark, 2016). Many experimental studies have been invested in understanding the roles of distal enhancers in regulating transcriptional bursting kinetics (Bartman et al., 2016; Chen et al., 2018; Fukaya et al., 2016; Rodriguez et al., 2019). However, the mechanism of how 3D chromatin organization (in particular 3D enhancer-promoter (E-P) spatial communication) in 1D time shapes transcriptional bursting patterns still remains elusive.

Hierarchic genomic structures captured by chromosome conformation capture and fluorescence *in situ* hybridization as well as other experimental technologies have provided evidence for supporting various possible E-P topologies and linking upstream distinctive E-P communications to downstream gene transcription (Bohrer and Larson, 2021; Gizzi et al., 2019; Li et al., 2020; Ou et al., 2017; Su et al., 2020). Measurable sustained physical proximity of E-P communication, which is believed to increase the local concentrations of transcription factors (TFs) and coactivators, seems necessary for cells to execute correct gene transcription programs in living *Drosophila* embryos (Chen et al., 2018; Lim et al., 2018). To understand the mechanism of transcriptional bursting theoretically, many gene models have been proposed, including simple models (e.g., the common ON-OFF model) (Corrigan et al., 2016; Kumar et al., 2014; Shahrezaei and Swain, 2008; Wang et al., 2020; Zhang and Zhou, 2019) and multistate models that seem good candidates for mimicking complex promoter dynamics in mammalian cells (Harper et al., 2011; Jones et al., 2014; Neuert et al., 2013; Rodriguez et al., 2019; Suter et al., 2011; Zhang and Zhou, 2014). However, these models ignore dynamic transcriptional regulation by spatial chromosome topology (Brouwer and Lenstra, 2019; Dekker and Mirny, 2016; Sood and Misteli, 2022). To the best of our knowledge, a comprehensive theory of the information transmission from upstream chromatin organization to downstream transcriptional bursting is still lacking. And important yet fundamental questions such as how E-P communication shapes the observed patterns of mRNA expression and what is the role of the “range of action” for E-P proximity in the control of bursting kinetics remain unsolved. Understanding and revealing transcriptional bursting kinetics characterized by burst size (BS) and burst frequency (BF) require integrative models that consider both 3D chromatin motion (including E-P spatial communication) and upstream-to-downstream regulation.

A collection of experimental evidence has firmly established that the E-P communication strength can significantly raise transcriptional levels (Bartman et al., 2019; Bartman et al., 2016; Senecal et al., 2014), e.g., the *sna* distal shadow enhancer generates more bursts than the primary enhancer in *Drosophila* embryos (Fukaya et al., 2016). Recent live-imaging measurements have provided clear evidence that E-P

genomic distance can effectively control gene activities and thus affect transcriptional bursting kinetics (Fukaya et al., 2016; Yokoshi et al., 2020; Zuin et al., 2022). These experimental observations indicate that the E-P communication strength limiting the E-P spatial distance and the E-P genomic distance arranged by chromosomal rearrangements are important factors impacting transcriptional bursting patterns. Currently, a new trend is that genomic structures are stochastic at almost every level of organization and this stochasticity is suggestively linked to gene transcription and finally affects transcriptional outcomes (Bohrer and Larson, 2021; Hübner et al., 2013; Sood and Misteli, 2022). Given the important impacts of these factors on transcriptional bursting, an unsolved and even theoretically unexplored issue is what principles govern transcriptional bursting kinetics. How E-P spatial and genomic distances differently influence BS and/or BF is unclear, either. As a matter of fact, biological systems are by nature multiscale. To date, many experimental studies have shown distinct timescale differences between upstream chromatin dynamics and downstream bursting kinetics (Johnstone et al., 2020; Lammers et al., 2020). For instance, E-P communication occurs on a timescale of seconds to minutes (Chen et al., 2018; Heist et al., 2019; Lim et al., 2018), whereas half-lives of Pol II pause during transcription on a timescale of minutes to hours (Henriques et al., 2018; Krebs et al., 2017; Shao and Zeitlinger, 2017). This temporal disconnection between the upstream and the downstream as well as the stochasticity of genomic organization and transcriptional bursting lies at the heart of a broad challenge in physical biology of forecasting transcriptional outcomes from the dynamics of underlying molecular processes.

Building upon experimental phenomena and data, we develop a generic theoretical framework to investigate how E-P communication affects transcriptional bursting kinetics, focusing on the uncovering of underlying molecular processes and dynamical mechanisms. This framework, which is formulated as a so-called 4D nucleome equation (similar to the classical differential Chapman-Kolmogorov Equation (Gardiner, 2004) in form), considers upstream chromatin motion on a fast timescale and downstream mRNA bursty production on a slow timescale as well as the connection between the upstream and the downstream (referring to Figure 1). We employ the 4D nucleome equation to analyze dynamic behaviors of transcriptional bursting across space and time, i.e., 4D transcriptional bursting kinetics (Dekker et al., 2017; Marti-Renom et al., 2018). Both model analysis and numerical simulations reveal fundamental principles of the E-P spatial communication in transcriptional bursting, mainly including two universal laws: E-P communication strength up-regulates BF and BS by power laws with positive exponents, and E-P genomic distance down-regulates bursting kinetics by power laws with negative exponents. In addition, we analytically show that E-P spatial distances follow a Maxwell-Boltzmann distribution. The theoretically predicted results are in accordance with experimental data. We emphasize that our model, which exhibits scalability by interpreting many experimental phenomena reported in the existing literature (Fukaya et al., 2016; Zuin et al., 2022), provides a generic modeling framework for studying how chromatin dynamics affect transcriptional bursting kinetics in realistic cases.

Results

The first principle framework of gene transcriptional bursting

Transcription involving multiple steps is driven mainly by E-P communication (Figure 1A and 1B), often exhibiting a burst-like pattern. Our goal is to develop a generic theoretical framework that can reveal the essential mechanism of transcriptional bursting and predict possible dynamic behaviors compatible with experimental observations. This framework considers that upstream chromatin dynamics play on a fast timescale and downstream transcriptional bursting operates on a relatively slow timescale, but keeps the upstream and the downstream linked via a biologically reasonable way.

First, based on Figures 1C-E, we can derive the following 4D nucleome equation (see Methods)

$$\frac{\partial \boldsymbol{p}(\boldsymbol{r},\boldsymbol{s};t)}{\partial t}=-\nabla_{\boldsymbol{r}}\cdot\left(\boldsymbol{p}(\boldsymbol{r},\boldsymbol{s};t)\boldsymbol{V}(\boldsymbol{r},\boldsymbol{s};t)^{\mathrm{T}}\right)+\nabla_{\boldsymbol{r}}^{2}\left(\boldsymbol{D}\boldsymbol{p}(\boldsymbol{r},\boldsymbol{s};t)\right)+\boldsymbol{W}(\boldsymbol{r};t)\,\boldsymbol{p}(\boldsymbol{r},\boldsymbol{s};t). \quad [1]$$

Here the column vector $\boldsymbol{p}(\boldsymbol{r},\boldsymbol{s};t)$ represents the joint probabilities that the positions of N nucleosomes are $\boldsymbol{r}$ and the gene states are $\boldsymbol{s}$ at time t; $\nabla_{\boldsymbol{r}}$ and $\nabla_{\boldsymbol{r}}^{2}$ are gradient and Laplace operators respectively; $\boldsymbol{V}(\boldsymbol{r},\boldsymbol{s};t)^{\mathrm{T}}$ (T: transpose) represents the deterministic velocity field for chromatin spatial motion; $\boldsymbol{D}$ is a diffusion matrix associated with chromatin stochastic motion under isotropic diffusion with diffusional coefficient D; and $\boldsymbol{W}(\boldsymbol{r};t)$ is the nucleosome position-dependent transition matrix for all gene states (Figure 1F). The first term on the right-hand side of Eq. [1] represents a deterministic component modeling the upstream chromatin motion and the second term represents a stochastic component accounting for random fluctuations, both altogether describing the chromatin's spatiotemporal diffusional process. The last term captures the gene states' randomly switching process driven by molecular events such as chromatin remodeling, TFs binding, and Pol II cluster. We point out that Eq. [1] seems the first theoretical model that comprehensively considers the connection between the upstream and the downstream molecular processes, and can be taken as a good starting point for analyzing how chromatin motion (including E-P communication) affects transcriptional bursting in complex cases.

Second, from a physical viewpoint, upstream chromatin can be modeled as a polymer discretized into a collection of successive monomers connected by harmonic spring (Doi et al., 1988). Both the promoter and enhancer in chromatin are regarded as monomers, and spatial communication exists between them. Chromatin motion involving E-P communication then evolves according to the Langevin equation $\mathrm{d}\boldsymbol{r}=\boldsymbol{V}(\boldsymbol{r},\boldsymbol{s};t)\mathrm{d}t+\sqrt{2D}\mathrm{d}\boldsymbol{B}(t)$ that is derived from Eq. [1], where $\boldsymbol{B}(t)$ is a vector of independent Brownian motions. We assume that changes in the gene state do not affect chromatin motion. Therefore, $\boldsymbol{V}(\boldsymbol{r},\boldsymbol{s};t)$ can be approximated as $\boldsymbol{V}(\boldsymbol{r};t)=-\nabla_{\boldsymbol{r}}U(\boldsymbol{r};t)/\gamma$, where $U(\boldsymbol{r};t)$ is the total potential of chromatin conformation and γ is a friction coefficient. $U(\boldsymbol{r};t)$ can be decomposed into $U(\boldsymbol{r};t)=U_{\mathrm{NN}}(\boldsymbol{r};t)+U_{\mathrm{EP}}(\boldsymbol{r};t)$, where $U_{\mathrm{NN}}(\boldsymbol{r};t)$ is the potential for the whole chain and is set as $(1/2)\sum_{j=1}^{N-1}k_{\mathrm{NN}}\left(\boldsymbol{r}_{j}-\boldsymbol{r}_{j+1}\right)^{2}$ with k_{NN} being the common spring coefficient, and $U_{\mathrm{EP}}(\boldsymbol{r};t)$ is the potential for E-P communication and is set as $(1/2)k_{\mathrm{EP}}\left(\boldsymbol{r}_{\mathrm{E}}-\boldsymbol{r}_{\mathrm{P}}\right)^{2}$ with $\mathrm{E},\mathrm{P}\in\{1,\cdots,N\}$ being the positions of the enhancer and promoter along the DNA

line respectively. Here k_{EP}, the ratio of the force generated by the biomolecule's interaction involved in E-P communication per unit of E-P spatial distance, represents E-P communication strength, reflecting E-P encounter frequency (Figure 1C, Supplemental Text A). k_{EP} cannot be directly measured by experiments but can be estimated from experimental data, e.g., Hi-C data (Lu et al., 2020). We point out that Lennard-Jones potential can also be used to simulate E-P communication, but does not affect the qualitative results to be obtained (Supplemental Fig S1F).

Downstream transcription apparatus can be characterized by promoter-state switching (Figure 1E). To reveal the essential mechanism of how E-P communication regulates transcriptional bursting, we introduce a minimal architecture for gene states – a four-state model (see Methods, and Supplemental Table S1) although more complex architectures are possible. In this model, a deep inactive state ($\mathrm{S}_{\mathrm{off2}}$) and a primed but inactive state ($\mathrm{S}_{\mathrm{off1}}$), both being integrated as OFF state, are used to explain chromatin remodeling and TF binding. Pol II recruitment state ($\mathrm{S}_{\mathrm{rec}}$, (Fuda et al., 2009)) and Pol II pause release state ($\mathrm{S}_{\mathrm{rel}}$, (Chen et al., 2017)), two critical processes involved in transcriptional bursting, are taken as ON state, and mRNA generation is accompanied by the transition from $\mathrm{S}_{\mathrm{rel}}$ to $\mathrm{S}_{\mathrm{rec}}$. If states $\mathrm{S}_{\mathrm{rel}}$ and $\mathrm{S}_{\mathrm{rec}}$ switch multiple times during one ON period, transcription will occur in a burst-like manner. The state transition matrix $\boldsymbol{W}$ in Eq. [1] consists of gene-state switching rates.

After identifying the above formulations, we build a link in terms of the information flow from upstream to downstream (Figure 1D), where E-P communication carries the upstream information to orchestrate bursting patterns, and downstream transition rates change accordingly. Specifically, we take E-P spatial distance d_{S} as an input and d_{S}-dependent gene-state switching rates as outputs (see Methods), thus bridging the upstream and the downstream. Although how E-P communication ways are implemented is arguing (Lim and Levine, 2021), E-P proximity has been believed to increase the likelihood of transcription bursting. In general, the smaller E-P distance is, the larger are switching rates $\boldsymbol{\lambda} = [\lambda_{\mathrm{on1}}, \lambda_{\mathrm{rec}}, \lambda_{\mathrm{rel}}]^{\mathrm{T}}$ whereas the smaller are transcriptional termination rates $\boldsymbol{\lambda}' = [\lambda_{\mathrm{off1}}, \lambda_{\mathrm{off2}}]^{\mathrm{T}}$. We assume that $\boldsymbol{\lambda}$ depends on E-P distance and $\boldsymbol{\lambda}'$ is independent of this distance. Since Hill function is very successful in modeling biological phenomena (Goutelle et al., 2008), we further suppose that $\boldsymbol{\lambda}$ is a Hill-like function vector $\boldsymbol{H}$ of d_{S} (see Methods). These assumptions would be idealistic for elaborate organisms, but all the settings constitute an analysis framework, which can be easily extended to more complex cases of transcriptional regulation.

We develop both an effective analytical approach and a numerical simulation algorithm (see Methods), to solve the entire system described by Eq. [1]. These methods provide a systematic approach for tracing the respective contributions of system's key parameters (e.g., E-P communication strength, E-P genomic distances) to the experimentally observable patterns of transcriptional bursting and further for revealing the essential mechanism of bursting kinetics.

Distribution characteristics of transcriptional bursting

In order to see the distribution characteristics of transcriptional bursting kinetics characterized by BS (defined as the number of mRNA molecules produced per burst) and BF (defined as the reciprocal of the cycle time (CT) that is defined as the total time that the gene dwells at OFF and ON states), we mainly find the BS distribution $p_{BS}(m)$ and the CT distribution $p_{CT}(t)$. Note that BS and CT depend on the E-P spatial distance d_S, which is a random variable following the distribution denoted by $p_{DS}(d_S)$ (Figure 1G). Before presenting results on $p_{BS}(m)$ and $p_{CT}(t)$, we derive the expression of $p_{DS}(d_S)$.

We analytically find that d_S obeys the following exact Maxwell-Boltzmann distribution (see Supplemental Text B and Supplemental Fig S1A)

$$p_{DS}(d_S) = \sqrt{\frac{2}{\pi}}\Theta^{-3} d_S^2 \exp\left(-\frac{d_S^2}{2\Theta^2}\right), \quad [2]$$

where $\Theta = \sqrt{D\gamma\left(k_{NN}/d_G + k_{EP}\right)^{-1}}$, which is a compound parameter depending on the genomic property, clearly defines an analytical relationship between E-P spatial distance d_S and E-P communication parameters (including E-P communication strength k_{EP} or E-P genomic distance d_G). Term $k_{NN}/d_G + k_{EP}$ actually represents the integrative effect of two paralleling springs, possibly hinting the principle of engineering communication between regulatory elements. Quantitative measurements of the distance between *Sox2* and its essential enhancer in living mouse embryonic stem cells (Supplemental Fig S1B, or see (Alexander et al., 2019)) and the distance between the *eve* locus and its enhancer in fly embryo (Brueckner et al., 2023) have indicated the validity of this Maxwell-Boltzmann distribution. Eq. [2] also uncovers a power-law behavior between encounter probabilities and E-P spatial (or genomic) distance, which is in accordance with experimental data for consecutive and nonconsecutive TAD borders in *Drosophila* (Supplemental Fig S1E, or seeing (Cattoni et al., 2017)).

We can also derive the expressions of two distributions $p_{BS}(m)$ and $p_{CT}(t)$, seeing Methods for details. Then, we find that if the gene-state switching rates are independent of d_S, BS follows a geometric distribution with the characteristic parameter representing the success probability of burst termination (Supplemental Text B); The duration of OFF period follows a bi-exponential distribution (Supplemental Text B), supporting that gene activation is not necessarily a one-step process following an exponential distribution (Harper et al., 2011; Kandhavelu et al., 2012; Suter et al., 2011); And the CT distribution is the weighted combination of multiple exponential distributions (Supplemental Text B), which demonstrates a non-origin peak. If the gene-state switching rates depend on d_S, $p_{BS}(m)$ or $p_{CT}(t)$ has no analytical expression but has an exactly approximate expression, i.e., Eq. [12] in Methods, which is derived by a timescale separation method that is due to the fast chromatin motion and the slow transcription reactions (Thomas et al., 2014).

We point out that in both cases, our approaches for deriving the analytical expressions of $p_{BS}(m)$ and $p_{CT}(t)$ can be applied to other more complex gene-transcription models. Thus all qualitative results are universal. In addition, parameter settings for the results demonstrated in the following several subsections

are put in Supplemental Table S2. Some parameters (e.g., those related to chromatin motion) are determined directly based on biological processes and physical equations, and others (e.g., transcriptional rates) are chosen based on theoretical analysis results and actual biological time scales (Supplemental Text F).

Transcriptional bursting kinetics follow power laws

How E-P communication modulates BS and BF is not only a debating biological issue but also an unsolved theoretical issue. Here we use the above arsenal of theoretical analysis to explore the qualitative impact of E-P communication strength k_{EP} on transcriptional bursting kinetics (i.e., BS and BF). As one of the most common modular organisms, *Drosophila* has been extensively studied in terms of bursting (Douglas, 2018; Jennings, 2011). Indeed, distinctive enhancers such as *sna* shadow and *sna* primary enhancer in *Drosophila* that interact with cognate promoter may lead to different burst kinetics (Bothma et al., 2015; Fukaya et al., 2016; Perry et al., 2010). In our analysis, we take different values of k_{EP} to characterize the inherent behaviors of E-P interaction. Meanwhile, we make use of the fact that effective experimental means such as external hormone (Stavreva et al., 2015) or heavy metal stimulations (Murata et al., 1999) can make E-P communication stronger, i.e., k_{EP} becomes larger. To reveal the distinct effects of different k_{EP} on bursting kinetics, we keep E-P genomic distance fixed (Figure 2A).

Figure 2B depicts how changes in k_{EP} alter chromatin conformations and further affect bursting profiles. Theoretically, a larger (smaller) k_{EP} corresponds to a shorter (longer) E-P spatial distance, and then the increasing k_{EP} can boost both BS and BF (Supplemental Figs. S1C and S4A-B). These features have been qualitatively supported by experimental evidence from different organisms (Bartman et al., 2019; Bartman et al., 2016; Fritzsch et al., 2018; Fukaya et al., 2016). Since ON state dwell-time remains fundamentally the same, the amplified BF can be achieved by progressively reducing OFF state dwell-time (Supplemental Fig S4C-D, (Fritzsch et al., 2018; Larson et al., 2013; Rodriguez et al., 2019)). This implies that the gene state switching rate λ_{on1}, associated with TF recruitment in biology, is a principal parameter affecting BF, in agreement with the experimental finding that a higher TF level leads to a higher BF on the c-Fos gene (Senecal et al., 2014).

To reveal the qualitative relevance of bursting kinetics to E-P communication strength, we further analyze two logarithmic gains $\partial \log_{10} \mathrm{BS} / \partial \log_{10} k_{\mathrm{EP}}$ and $\partial \log_{10} \mathrm{BF} / \partial \log_{10} k_{\mathrm{EP}}$ (i.e., two partial derivatives), which measure how BS and BF are affected by k_{EP}. Binary approximations of gene-state switching rates provide a good strategy for simplifying analysis including estimating BS and BF (see Methods, Supplemental Figs. S5D-E). The detailed theoretical analysis shows that the logarithmic gains are about zero when k_{EP} is too small ($k_{\mathrm{EP}} < 0.01$) or too large ($k_{\mathrm{EP}} > 1$) (Supplemental Figs. S5A-C), implying that transcriptional burst response is insensitive to k_{EP} in these two cases. Then we focus on a reasonable biological range of k_{EP} (e.g., $0.01 < k_{\mathrm{EP}} < 1$). The logarithmic gains are almost constant and BS and BF can be thus approximated with linear functions of k_{EP} on a logarithmic scale (Figures 2C-D and

Supplemental Figs. S5D-E). Concretely, for $0.01 < k_{EP} < 1$, BS and BF approximately obey the following power-law behaviors

$$\text{burst size} \sim (k_{EP})^{S_{BS}}, \quad \text{burst frequency} \sim (k_{EP})^{S_{BF}}, \qquad [3]$$

where S_{BS} and S_{BF} are two positive scaling exponents that can be theoretically estimated (see Methods). Note that these two different scaling exponents, e.g., $S_{BS} = 0.23$ in Figure 2C and $S_{BF} = 0.30$ in Figure 2D, are critical indices since they reflect the ability of BS and BF responses to E-P communication, which will be detailedly analyzed in the next section. To ascertain whether the power-law behaviors shown in Eq. [3] always hold, we change key parameters in broad ranges. For all possible cases of parameter values, we find that log-log plots between BS (or BF) and k_{EP} still demonstrate an approximately linear relationship, implying that the growing tendency can still be featured by power-law relationships (Supplemental Fig S6).

The above theoretical predictions have been verified by experimental data. Based on the BF data (converted the unit into sec^{-1}) for different enhancers in living *Drosophila* embryos (Fukaya et al., 2016) and the above model, we theoretically infer the E-P communication strength for each enhancer and calculate the mean mRNA (which approximately equals to the product of BS and BF (Li et al., 2021)). We find that the mRNA level matches well with the experimental results (Fluorescence intensity is a relative value, converting its trend of change into a fold change) and both the BF and mRNA levels show power-law relationships in logarithmic coordinates (Figures 2E-F). Our results not only demonstrate the ability of our model in explaining and predicting the experimental data, but also further prove the validity of the power-law theoretical results.

E-P communication mainly modulates burst frequency rather than burst size

Note that Eq. [3] indicates that BS and BF regulated by E-P communication strength k_{EP} follow their own power-law behaviors. Since S_{BS} and S_{BF} in Eq. [3] reflect the regulation ability of k_{EP}, we next compare the sizes of S_{BS} and S_{BF}, i.e., compute the ratio of S_{BF}/S_{BS}, to show which of the BS and BF is primarily regulated by E-P communication. For this goal, we change E-P communication strength and all gene-state switching rates in broad ranges. In general, extracting insights from directly analyzing the effects of these changes in high-dimensional parameter space consisting of E-P communication strength and all gene-state switching rates on BS and BF is very difficult. Therefore, we resort to a dimension reduction method that maps a high dimensional parameter space into an experimentally measurable and theoretically computable two-dimensional space (Figure 3A) in which two indices ρ_{BS} and ρ_{BF} are defined as the ratios of the maximum BS and BF over the minimum BS and BF, respectively (see Supplemental Text D).

Next, we calculate ratio S_{BF}/S_{BS} in the (ρ_{BF}, ρ_{BS}) space. Note that one point in the low-dimensional space possibly corresponds to multiple points in the high-dimensional space due to the irreversibility of the mapping. To overcome this multiple-to-one difficulty, we use the averaging method to estimate the

ratio S_{BF}/S_{BS}, and then find that this ratio generally increases with the growth of ρ_{BF} or with the shrinking of ρ_{BS} (Figure 3A and Supplemental Fig S7A). In Figure 3B, the separatrix $S_{BF}/S_{BS}=1$ (red line) separates the space into two regions: upper $S_{BF}>S_{BS}$ and lower $S_{BF}<S_{BS}$. In particular, the data shown in Figures 2C and 2D corresponds to the point $(\rho_{BF},\rho_{BS})=(5.8,3.1)$, which apparently locates in the area of $S_{BS}<S_{BF}$ ($S_{BF}/S_{BS}=1.4$, Figure 3B, red-blue mixed circle). To show the reliability of this averaging method, we use the minimum (or maximum) value rather than the mean to compute S_{BF}/S_{BS}. As a result, the separatrix $S_{BF}/S_{BS}=1$ displays a similar changing trend, i.e., the range of the ρ_{BS} satisfying $S_{BS}<S_{BF}$ gradually becomes larger with the increase of ρ_{BF} (Supplemental Fig S7B).

To complete the above analysis, we consider enhancer deletion where k_{EP} is exactly zero (Supplemental Fig S2A). For the same parameter values as in the above calculation, we find that the sizes of ρ_{BS} and ρ_{BF} with enhancer deletion are the same as those with enhancer regulation but the slope ratio $S_{BF}^{E}/S_{BS}^{E}(=1.56)$ (representing the ratio after enhancer deletion, Supplemental Text D) is different from the value of $S_{BF}/S_{BS}(=1.4)$ (Figure 3B, red-blue mixed circle). Using the results obtained by a similar method of calculating S_{BF}/S_{BS}, we draw the separatrix $S_{BF}^{E}/S_{BS}^{E}=1$ in Figure 3B (blue line). Then we find that whether enhancer deletion is considered does not influence ρ_{BS} and ρ_{BF}, but impacts ratios S_{BF}/S_{BS} and S_{BF}^{E}/S_{BS}^{E} (referring to two different oblique lines in Supplemental Fig S2F).

Finally, we locate the experimental data into the (ρ_{BF},ρ_{BS}) space and determine which of BS and BF is mainly regulated by E-P communication. Although experimental data on gene-state switching rates are lacking, we may use the maximum and minimum BS and BF experimentally available to compute ρ_{BS} and ρ_{BF}. Since we integrate the model parameters into two experimentally measurable and theoretically computable quantities, the validation of model predictions does not require a specific data set. Based on analysis of data from transgene experiments, we find that the MS2 reporter gene displays different bursting kinetics for different enhancer strengths, e.g., for a stronger *sna* shadow enhancer and a weaker *Kr* CD2 enhancer, the result is $(\rho_{BF},\rho_{BS})=(2.3,1.3)$ (Figure 3B, red square point, (Fukaya et al., 2016)). The maximum BS of the gene *β*-globin measured in an experiment of erythroid maturation is over three times the minimum gained by the deletion of the LCR enhancer (Figure 3B, dashed blue diamond point, (Bartman et al., 2016)). In addition, based on the *Sox2* gene expression data with and without enhancer deletion in normal ES cells, we can infer that the BS reduces 1.4 times and the BF reduces roughly 15 times (Figure 3B, blue triangle point, (Larsson et al., 2019b)). We find that all these analyzed experimental data are all located in a narrower region of $S_{BS}<S_{BF}$ (the right lower region in Figure 3B), further verifying that the E-P communication mainly modulates BF rather than BS.

Saturation effects of E-P genomic distance on bursting kinetics

Having devled into the qualitative effect of E-P communication strength k_{EP} on bursting kinetics as described in Eq. [3], we next analyze how E-P genomic distance d_G quantitatively impacts transcriptional activities and further bursting kinetics. To focus on the effect of d_G on BS and BF, we freeze k_{EP} but make d_G increase. This can be achieved by arranging the enhancer and the promoter symmetrically on

the chain and letting them move in the opposite direction along the chain (Figure 4A).

From Eq. [2], we see that d_{G} and k_{EP} have the just opposite impact on E-P spatial distance (Supplemental Figs. S1C). By the similar method of analyzing the effect of k_{EP} on BS and BF, we find that two logarithmic gains $\partial \log_{10} \mathrm{BS} / \partial \log_{10} d_{\mathrm{G}}$ and $\partial \log_{10} \mathrm{BF} / \partial \log_{10} d_{\mathrm{G}}$ are negative, implying that the increasing E-P genomic distance can reduce BS and BF (Supplemental Figs. S5F-H). With the further increase of d_{G}, both BS and BF finally reduce to constants. These analyses indicate that the responses of BS and BF to the E-P genomic distance exhibit first descent and then stable change tendencies if other system parameters are fixed (Figures 4B and 4C).

In order to confirm the saturation effects obtained by the above theoretical analysis, we first carry out numerical simulations and then perform the Kruskal-Wallis nonparametric test for simulated samples. This statistical test can identify the turning point of the responses of BS and BF to d_{G}. Here the turning point (referring to black dashed lines in Figures 4B and 4C) is defined as the value of d_{G} for which the Kruskal-Wallis test has no significant difference for the first time (referring to grey circles in Figures 4B and 4C). We denote the d_{G} values corresponding to the turning points of BS (BF) as $d_{\mathrm{G}}^{\mathrm{BS}}$ ($d_{\mathrm{G}}^{\mathrm{BF}}$).

Furthermore, we use functions to characterize the above saturation effects. The logarithmic gains of BS and BF are almost constant for d_{G} in the range of $d_{\mathrm{G}} \le d_{\mathrm{G}}^{\mathrm{BS}}$ or $d_{\mathrm{G}} \le d_{\mathrm{G}}^{\mathrm{BF}}$, implying that in this range, the logarithmic gains can be approximated as linear functions of d_{G}, or equivalently, BS and BF can be approximated as power functions of d_{G} with exponents ℓ_{BS} and ℓ_{BF} respectively (Supplemental Figs. S5I-J). In contrast, BS and BF are all constants in the range of $d_{\mathrm{G}} > d_{\mathrm{G}}^{\mathrm{BS}}$ or $d_{\mathrm{G}} > d_{\mathrm{G}}^{\mathrm{BF}}$. In summary, the change tendencies of BS and BF can be mathematically described as

$$\text{burst size} \sim \begin{cases} (d_{\mathrm{G}})^{\ell_{\mathrm{BS}}}, & d_{\mathrm{G}} \le d_{\mathrm{G}}^{\mathrm{BS}}, \\ const., & d_{\mathrm{G}} > d_{\mathrm{G}}^{\mathrm{BS}}, \end{cases} \quad \text{burst frequency} \sim \begin{cases} (d_{\mathrm{G}})^{\ell_{\mathrm{BF}}}, & d_{\mathrm{G}} \le d_{\mathrm{G}}^{\mathrm{BF}}, \\ const., & d_{\mathrm{G}} > d_{\mathrm{G}}^{\mathrm{BF}}. \end{cases} \qquad [4]$$

Here ℓ_{BS} and ℓ_{BF} are two negative scaling exponents that can be theoretically estimated. Note that these scaling exponents are in general different between BS (e.g., $\ell_{\mathrm{BS}} = -0.16$ in Figure 4D, red) and BF (e.g., $\ell_{\mathrm{BF}} = -0.19$ in Figure 4E, red). An intuitive explanation for the asymptotic trend in large d_{G} is that the lumping parameter $\Theta = \sqrt{D\gamma\left(k_{\mathrm{NN}}/d_{\mathrm{G}} + k_{\mathrm{EP}}\right)^{-1}}$ in Eq. [2] approaches to a constant with the enlargement of d_{G}, indicating that for sufficiently large d_{G}, the effect of E-P communication on transcriptional bursting is mainly determined by communication strength k_{EP} rather than by E-P genomic distance d_{G}.

The above saturation effects have been also verified by experimental results. First, quantitative living-imaging methods showed that a large E-P genomic distance between the *sna* shadow enhancer and its target gene significantly diminishes the levels of BS and BF in *Drosophila* (Fukaya et al., 2016; Yokoshi et al., 2020), in accordance with our prediction on what BS and BF are monotonically decreasing with increasing d_{G}. Second, the mRNA expression level, which approximately equals to the product of BS and the BF (Li et al., 2021), is an approximate linear function of smaller E-P genomic distance d_{G} on a logarithmic scale (Figure 4F, (Zuin et al., 2022)). Third, now that a monotonically decreasing transcription level does not drop to zero, the case that the level remains at a low level for large d_{G} could happen (Zuin et al., 2022). In a word, the E-P genomic distance impacts the mRNA expression level in a

piecewise power manner as described in Eq. [4].

Mutual information reveals the dependence of bursting kinetics on E-P communication

In the above sections, we have used the average method, i.e., calculating the mean BS and BF (the reciprocal of mean CT) that only considers the mean information of BS's and CT's distribution, to study the impact of E-P communication on bursting kinetics. Here, we investigate bursting kinetics from a perspective of information transmission. The signaling pathway of transcriptional regulation transmits upstream E-P communication signal distribution $p_{DS}(d_S)$ to downstream transcriptional output distribution $p_X(x)$ (Figure 5A). The noisy "promoter channel" limits the fidelity of this information transduction. To better understand the ability of E-P communication to regulate BS and BF, here we use Shannon mutual information to measure how much information about the E-P communication is decoded in bursting kinetics (Cover, 1999; Shannon, 1948). Mutual information $\mathrm{MI}(X,DS)$ measured in bits is defined as

$$\mathrm{MI}(X,DS)=\int_0^{+\infty}\int_0^{+\infty} p_{X,DS}(x,d_S)\log_2\left(\frac{p_{X,DS}(x,d_S)}{p_X(x)\,p_{DS}(d_S)}\right)\mathrm{d}x\mathrm{d}d_S\,, \qquad [5]$$

where $p_X(x)$ can represent BS distribution $p_{BS}(m)$, CT distribution $p_{CT}(t)$, OFF dwell-time distribution $p_{OFF}(t)$ and ON dwell-time distribution $p_{ON}(t)$, respectively (Supplemental Figs. S4). The mutual information defined in such a manner can capture the contributions of all the aspects of transcriptional output distributions, not just the mean values.

Based on the computation of $\mathrm{MI}(X,DS)$ in a wide range of k_{EP}, we find that $\mathrm{MI}(BS,DS)$ is much smaller than $\mathrm{MI}(CT,DS)$ (Figures 5B and 5C), implying that BF transmits more information than BS. Moreover, $\mathrm{MI}(ON,DS)$ is two-order smaller than $\mathrm{MI}(OFF,DS)$, indicating that ON dwell-time is insensitive when responding to the transduced information (Figure 5C, red dashed line). Additionally, all the $\mathrm{MI}(X,DS)$ in Figures 5B and 5C exhibit first increase and then decrease, indicating that the information transduction capacity is tunable and there exists an optimal k_{EP} that maximizes the $\mathrm{MI}(X,DS)$.

Note that the maximum mutual information (MMI) measures the maximum information transmission capacity over all possible signal distributions. Obviously, the MMI exists in Figures 5B and 5C, where $k_{\mathrm{EP}}=0.05$ for $\mathrm{MI}(BS,DS)$ and $k_{\mathrm{EP}}=0.07$ for $\mathrm{MI}(CT,DS)$. To ascertain whether or not such an optimal k_{EP} always exists, we change key parameters in wide ranges and find that there is indeed a critical k_{EP} maximizing the $\mathrm{MI}(X,DS)$ shown in Figures 5D and 5E and Supplemental Fig S8. In addition, the MMIs for BS and CT correspond to different k_{EP} values (see red lines in Figures 5D and 5E). This asynchronous maximization indicates that the signal transduction pathway is BS- or BF-specific. In particular, the observation that $\mathrm{MI}(DS,BS)$ is smaller than $\mathrm{MI}(DS,CT)$ in region II (Figures 5D and 5E, the region below the white line) indicates that BF transmits more E-P communication information than BS,

and consequently, E-P communication mainly regulates BF rather than BS.

Discussion

Imaging studies, high-resolution chromatin conformation maps, and genome-wide occupancy profiles of architectural proteins have revealed that genome topology encoding E-P communication information is tightly correlated with gene expression through complex regulatory layers, creating various possible transcriptional burst phenotypes. The prediction of these phenotypes requires a quantitative understanding of transcriptional bursting mechanisms underlying the influence of genomic architectures. In this paper, we have proposed a multiscale model, which integrates the 3D information on chromatin dynamics into transcription bursting, to shed light on the pivotal role of E-P spatial communication in the control of transcriptional bursting kinetics.

We have established a generic modeling framework that captures salient features of intra-nuclear transcriptional bursting processes. First, we use the generalized Rouse model, which can well describe chromatin motion including E-P communication, to model chromatin dynamics. Second, we use a four-state model of gene transcription to capture important events occurring in transcriptional processes. A special feature of our model is that it uses a change of gene state to model the simultaneous freeing of promoter sites and the production of mRNA due to unpausing of the promoter-proximal paused state (Braichenko et al., 2021; Cao et al., 2020; Karmakar, 2020; Karmakar and Das, 2021; Szavits-Nossan and Grima, 2023; Weidemann et al., 2023). This is crucial for capturing the feature that only one Pol II is permitted to bind to promoter and the second Pol II recruitment must occur after the first Pol II pause release. Also, our model can capture some characteristics (such as traveling ratio, the effect of altering Pol II pause release rate) that cannot be obtained by the previous models. Third, we use a function vector to link upstream chromatin configurations to downstream gene transcription. The function vector can be viewed as an information transmission process, which can be sensitive, insensitive, positively correlated, or negatively corrected. Different link functions can result in the distance being irrelevant or even anti-correlated with transcription to characterize distinctive experimental phenomena (Benabdallah et al., 2019). It is worth pointing out that more complex E-P topologies, transcription processes or/and link functions can be incorporated in our model, but the qualitative (but possibly quantitative) results including power-law behaviors and the preferential modulation of burst frequency demonstrated by theoretical derivation still hold.

Our analysis has given a clear answer to the question of which of BS and BF is modulated more than the other by E-P communication. In contrast to the transcriptome-wide inference that shows the important role of E-P communication in controlling BF (Larsson et al., 2019a; Larsson et al., 2019b; Ochiai et al., 2020), we have theoretically confirmed that enhancer mainly modulates BF rather than BS (Figure 3B), which is in agreement with observations of most experiments (Bartman et al., 2016; Fukaya et al., 2016; Larson et al., 2013; Sutherland et al., 1997; Walters et al., 1995; Zuin et al., 2022). Moreover, we have

given theoretical estimates on the effect of the enhancer on BF and BS, which is based on directly calculating the ratio of the maximum and minimum values of BS and BF experimental available. In addition, from the view of mutual information, we have shown that transcriptional bursting kinetics are regulated by transmitting more information to BF, which further verifies the importance of enhancers in modulating BF.

Our results allow us to make important predictions about how upstream chromatin dynamics affect downstream transcriptional bursting kinetics. First, we have shown that E-P communication strength k_{EP}, a key parameter in our model, up-regulates BS and BF in power-law manners with positive exponents. These power-law behaviors were verified by experimental data (Fukaya et al., 2016) and more experiments are still needed. Second, we have demonstrated that E-P genomic distance d_{G}, another vital parameter in our model, modulates BS and BF in saturating fashions. These saturation effects were also verified by recent experimental observations (Zuin et al., 2022). The opposite change trends for the effects of k_{EP} and d_{G} on bursting kinetics showed that the combination of k_{EP} and d_{G} would be a flexible regulation strategy that can provide insights into complex mechanisms of biological processes in organisms. In addition, the fact that different gene-state transition rates lead to different scaling exponents in power-law behaviors of BS and BF indicates that the regulatory logics shaping differential signal transduction pathways would be cell-specific and even gene-specific (Brivanlou and Darnell Jr, 2002). Third, using mutual information to measure how upstream E-P communication dynamically and stochastically regulates downstream transcriptional bursting kinetics would be a more reasonable way. We have shown that the promoter information transduction capacity is tunable, and the MMI can be obtained by adjusting E-P communication strength k_{EP}. Supplemental Text E gives the possible reasons for the small value of mutual information.

Recently, Xiao *et al.* (Xiao et al., 2021) and Zuin *et al.* (Zuin et al., 2022) studied the control of 3D structure (including E-P communication) to gene transcription in different manners. The former assumed that the E-P signal participated in the accumulation and removal of TFs conducive to transcription while ignoring the actual chromatin conformation. The latter used two discrete states (far and close) rather than a continuous random variable as considered in our model, to simulate the E-P interaction and impact the OFF to ON process in a multi-step process with cumulative effects. Our model's direct and dynamic regulation leads to the variable rate from $\mathrm{S}_{\mathrm{off2}}$ to $\mathrm{S}_{\mathrm{rec}}$, which can basically be considered an alternative way to the cumulative effect process. Thus, our model explicitly considered the continuous fluctuation of upstream chromatin and the discrete switching of promoter states in the 4D space.

Our results are not limited to specific genes in *Drosophila* but may be applied to other organisms. The experimental data from different organisms such as a mouse model can be also well-fitted (Figures 3 and 4F) (Bartman et al., 2016; Zuin et al., 2022), indicating the extensibility of our results. Owing to the lack of experimental data on chromatin conformation and transcription burst data of the same gene in different situations, more experiments are needed to confirm the theoretical predictions. Our modeling framework

can also be extended to more complex situations. For example, some experimental studies reported that transcription can affect chromatin structure (Busslinger et al., 2017; Heinz et al., 2018), and we can incorporate this feedback to our model by modifying the gene-state-dependent drift function $\boldsymbol{V}(\boldsymbol{r},\boldsymbol{s};t)$ in Eq. [1]. In addition, our modeling of chromatin motion is not limited to one pair E-P communication. The potential applications may include the cases of multiple enhancers to one promoter (He et al., 2014), one enhancer to multiple promoters (Fukaya et al., 2016), or super-enhancers (Pott and Lieb, 2015). Using multi-state models of gene expression to extract insights from enormous experimental data and complex biological phenomena is impressing. Our four-state model is not a default option, and we may adjust the form of the downstream transcription model to include more complex biological processes such as mRNA splices (Kan et al., 2002) and cell cycle (Johnson and Walker, 1999).

Finally, we point out that our theoretical model, which aims to develop a general modeling framework to study 4D transcriptional bursting kinetics, may provide an opportunity for a dialogue between theoretical studies and biological experiments. We envision that our modeling framework will be useful for biophysical analysis of broader in *vivo* cellular processes.

Methods

Derivation of 4D nucleome equation

Let $\boldsymbol{p}(\boldsymbol{r},\boldsymbol{s};t)$ be a vector of the joint probability density functions (PDFs) that nucleosomes are in position $\boldsymbol{r}=[\boldsymbol{r}_1,\cdots,\boldsymbol{r}_N]^{\mathrm{T}}$ and the gene is in state $\boldsymbol{s}=[s_1,\cdots,s_K]^{\mathrm{T}}$ at time t, where T is transpose. Note that $\boldsymbol{p}(\boldsymbol{r},\boldsymbol{s};t)=\left[\boldsymbol{p}(\boldsymbol{r},s_1;t),\cdots,\boldsymbol{p}(\boldsymbol{r},s_K;t)\right]^{\mathrm{T}}$ can be regarded as a mapping: $\mathrm{R}^{3N}\times S\times\mathrm{R}\mapsto\mathrm{R}^{K}$ where $S=\{s_1,\cdots,s_K\}$. $\boldsymbol{p}(\boldsymbol{r},\boldsymbol{s};t)$ can be written as the product of the PDF $p(\boldsymbol{r};t)$: $\mathrm{R}^{3N}\times\mathrm{R}\mapsto\mathrm{R}$ and the conditional PDF (cPDF) $\boldsymbol{p}(\boldsymbol{s}|\boldsymbol{r};t)=\left[\boldsymbol{p}(s_1|\boldsymbol{r};t),\cdots,\boldsymbol{p}(s_K|\boldsymbol{r};t)\right]^{\mathrm{T}}: S\times\mathrm{R}\mapsto[0,1]^{K}$. That is $\boldsymbol{p}(\boldsymbol{r},\boldsymbol{s};t)=p(\boldsymbol{r};t)\,\boldsymbol{p}(\boldsymbol{s}|\boldsymbol{r};t)$. Differentiating it with respect to time yields

$$\frac{\partial\boldsymbol{p}(\boldsymbol{r},\boldsymbol{s};t)}{\partial t}=\frac{\partial p(\boldsymbol{r};t)}{\partial t}\boldsymbol{p}(\boldsymbol{s}|\boldsymbol{r};t)+\frac{\partial\boldsymbol{p}(\boldsymbol{s}|\boldsymbol{r};t)}{\partial t}p(\boldsymbol{r};t). \qquad [6]$$

Considering that $\boldsymbol{r}\in\Omega\subset\mathrm{R}^{3N}$ is a "fast" variable for a continuous trajectory, where Ω is a connected and bounded domain. Then, $\partial p(\boldsymbol{r};t)/\partial t$ in Eq. [6] can be formally written as $\partial p(\boldsymbol{r};t)/\partial t=-\nabla_{\boldsymbol{r}}\cdot\boldsymbol{J}(\boldsymbol{r},\boldsymbol{s};t)$, where $\nabla_{\boldsymbol{r}}$ is the gradient operator, $\boldsymbol{J}(\boldsymbol{r},\boldsymbol{s};t)=\boldsymbol{F}(\boldsymbol{r},\boldsymbol{s};t)\,p(\boldsymbol{r};t)$ is the probability flux and $\boldsymbol{F}(\boldsymbol{r},\boldsymbol{s};t)$ is a velocity field. If we only consider isotropic diffusion and friction, then $\boldsymbol{F}(\boldsymbol{r},\boldsymbol{s};t)$ can take the generalized Fokker–Planck approximation $\boldsymbol{F}(\boldsymbol{r},\boldsymbol{s};t)=\boldsymbol{V}(\boldsymbol{r},\boldsymbol{s};t)-\nabla_{\boldsymbol{r}}\left(D\log p(\boldsymbol{r};t)\right)$, where D is a diffusion coefficient. If we assume that changes in gene state do not contribute to chromatin motion, the velocity field $\boldsymbol{V}(\boldsymbol{r},\boldsymbol{s};t)$ can be approximated by $\boldsymbol{V}(\boldsymbol{r};t)$. Then,

$$\frac{\partial p(\boldsymbol{r};t)}{\partial t}=-\nabla_{\boldsymbol{r}}\cdot\left(\boldsymbol{V}(\boldsymbol{r};t)\,p(\boldsymbol{r};t)\right)+\nabla_{\boldsymbol{r}}^{2}\left(Dp(\boldsymbol{r};t)\right), \qquad [7]$$

where the first term represents the deterministic part and the second term is a stochastic ingredient of the velocity field.

On the other hand, consider that gene state $\boldsymbol{s}$ is a "slow" variable in a discrete pathway. Then,

$\partial \boldsymbol{p}(\boldsymbol{s}|\boldsymbol{r};t)/\partial t$ features the process of gene-state switching, and can be written by a master equation:

$$\frac{\partial \boldsymbol{p}(\boldsymbol{s}|\boldsymbol{r};t)}{\partial t} = \boldsymbol{W}(\boldsymbol{r};t)\,\boldsymbol{p}(\boldsymbol{s}|\boldsymbol{r};t), \quad [8]$$

where $\boldsymbol{W}(\boldsymbol{r};t) = \left(\lambda_{ij}(\boldsymbol{r};t)\right)_{K\times K}$ is a nucleosome position-dependent state transition matrix, satisfying the conservative condition: $\sum_{i=1}^{K}\lambda_{ij}(\boldsymbol{r};t) = 0$.

We assume that tiny changes in nucleosome coordinates do not alter gene state, implying that the derivative of conditional probability, $\nabla_{\boldsymbol{r}}\boldsymbol{p}(\boldsymbol{s}|\boldsymbol{r};t)$, approximately equals zero partly because of the time interval of downstream gene state transition is generally longer than that of upstream chromatin motion (Lammers et al., 2020). Then substituting Eq. [7] and Eq. [8] into Eq. [6] and using the assumption yield Eq. [1].

Since we are interested in the effect of E-P communication on transcriptional bursting when the system is at a steady state (or after a long time), the initial conditions of Eq. [1] become not so important. Meanwhile, since the chromatin chain is moving stochastically in a restricted nucleus space, reflecting boundaries of Eq. [1] exist theoretically. However, since our model only focuses on the local structural dynamics of a segment of chromatin, we do not need to consider the behaviors of local motifs at the nuclear membrane boundary and assumed that the boundary condition is a free boundary.

Simulation algorithm of 4D nucleome equation

Due to the coupling of the E-P communication and gene expression, we propose an algorithm to simulate the time evolution of the entire system.

Assume that there are L reactions involved in the gene-state switching process. The l-th reaction propensity is denoted by $a_l(\boldsymbol{r},\boldsymbol{s};t)$, $l = 1,2,\cdots,L$, and the total reaction propensity is calculated according to $a_{\text{tot}}(\boldsymbol{r},\boldsymbol{s};t) = \sum_{l=1}^{L} a_l(\boldsymbol{r},\boldsymbol{s};t)$. Note that $\boldsymbol{s}$ is the vector of all gene states, but in the following algorithm, we set K-dimensional state vector $\boldsymbol{s} = \left[0,\cdots,0,\underset{j\text{-th}}{1},0,\cdots,0\right]^{\mathrm{T}}$ when the current state is j in numerical simulation. Element v_{ij} of stoichiometric matrix $\left(v_{ij}\right)_{K\times L}$ denotes the net change in gene state j due to each reaction i, and $\boldsymbol{v}_{\mu}$ is the μ th column of $\left(v_{ij}\right)$. Let $H(\boldsymbol{r},\boldsymbol{s};t)$ is the survival probability that chromatin position is $\boldsymbol{r}$ and gene state is $\boldsymbol{s}$ state at time t. The main steps for solving Eq. [1] are listed below:

(1) Set the initial state as $\boldsymbol{r}_0 = \boldsymbol{r}(t_0)$, $\boldsymbol{s}_0 = \boldsymbol{s}(t_0)$.

(2) Generate two random variables u_1 and u_2 distributed uniformly in interval $(0,1)$.

(3) Integrate the system of stochastic differential equations

$$\begin{cases} \mathrm{d}\boldsymbol{r} = \boldsymbol{V}(\boldsymbol{r};t)\mathrm{d}t + \sqrt{2\boldsymbol{D}}\mathrm{d}\boldsymbol{B}(t), \\ \mathrm{d}H(\boldsymbol{r},\boldsymbol{s};t) = -a_{\text{tot}}(\boldsymbol{r},\boldsymbol{s};t)H(\boldsymbol{r},\boldsymbol{s};t)\mathrm{d}t, \\ \boldsymbol{r}(t_i) = \boldsymbol{r}_i,\ H(t_i) = 1, \end{cases}$$

from time points t_i to $t_i + \tau_i$, and with the stopping condition $H(\boldsymbol{r}_i,\boldsymbol{s}_i;t_i+\tau_i) = u_1$.

(4) Update time and position: $t_{i+1} = t_i + \tau_i$, $\boldsymbol{r}_{i+1} = \boldsymbol{r}(t_{i+1})$.

(5) Choose μ such that

$$\sum_{l=1}^{\mu-1} a_l\left(\boldsymbol{r}_{i+1}, \boldsymbol{s}_i; t_{i+1}\right) < u_2 a_{\mathrm{tot}}\left(\boldsymbol{r}_{i+1}, \boldsymbol{s}_i; t_{i+1}\right) \le \sum_{l=1}^{\mu} a_l\left(\boldsymbol{r}_{i+1}, \boldsymbol{s}_i; t_{i+1}\right).$$

(6) Update promoter state: $\boldsymbol{s}_{i+1} = \boldsymbol{s}_i + \boldsymbol{v}_\mu$.

(7) Reiterate the system from step (2) with a new state until a given largest time $t_{\max}$ is reached.

By the above algorithm steps, we can generate sample trajectories of the system.

Details of transcription model

The downstream bursting system to be studied is described by a set of biochemical reactions on a slow timescale in contrast to the chromatin motion on a fast timescale

$$\begin{aligned}
&\text{Chromatin opening:} && \mathrm{S_{off2}} \xrightarrow{\lambda_{\mathrm{on2}}} \mathrm{S_{off1}},\\
&\text{Chromatin closure:} && \mathrm{S_{off1}} \xrightarrow{\lambda_{\mathrm{off2}}} \mathrm{S_{off2}},\\
&\text{Burst initiation:} && \mathrm{S_{off1}} \xrightarrow{\lambda_{\mathrm{on1}}} \mathrm{S_{rec}},\\
&\text{Pol II recruitment:} && \mathrm{S_{rec}} \xrightarrow{\lambda_{\mathrm{rec}}} \mathrm{S_{rel}},\\
&\text{Pol II pause release:} && \mathrm{S_{rel}} \xrightarrow{\lambda_{\mathrm{rel}}} \mathrm{S_{rec}} + \mathrm{mRNA},\\
&\text{Burst termination1:} && \mathrm{S_{rec}} \xrightarrow{\lambda_{\mathrm{off1}}^{\mathrm{rec}}} \mathrm{S_{off1}},\\
&\text{Burst termination2:} && \mathrm{S_{rel}} \xrightarrow{\lambda_{\mathrm{off1}}^{\mathrm{rel}}} \mathrm{S_{off1}}.
\end{aligned}$$

The details and rationality of the model are shown in Supplemental Text A.

Many biological processes require the participation of E-P communication (or the enhancer, Supplemental Table S1). For example, enhancers recruit Mediator complex or histone acetyltransferase p300 to help the Pol II on promoters initiate transcription (Haberle and Stark, 2018). Enhancers promote the dissociation of NELF by recruiting COFs to affect Pol II pause-release on promoter-proximity (Aoi et al., 2020). Therefore, we assume the state-switching rate vector $\boldsymbol{\lambda}$ (consisting of λ_c, $c \in \{\mathrm{on1,rec,rel}\}$) depends nonlinearly on the E-P spatial distance d_{S} and assumes $\boldsymbol{\lambda} = \boldsymbol{H}(d_{\mathrm{s}})$. The variable λ_c depending on the E-P spatial distance is

$$\lambda_{\mathrm{c}}(d_{\mathrm{S}}) = \begin{cases} \lambda_{\mathrm{c,max}}, & d_{\mathrm{S}} \le \varepsilon_{\mathrm{T}}, \\ \lambda_{\mathrm{c,min}} + \left(\lambda_{\mathrm{c,max}} - \lambda_{\mathrm{c,min}}\right) \Big/ \left[1 + \left(\dfrac{d_{\mathrm{S}} - \varepsilon_{\mathrm{T}}}{\varepsilon_{1/2} - \varepsilon_{\mathrm{T}}}\right)^h\right], & d_{\mathrm{S}} > \varepsilon_{\mathrm{T}}, \end{cases} \qquad [9]$$

where $\lambda_{\mathrm{c,min}}$ and $\lambda_{\mathrm{c,max}}$ are the minimum (basic) and maximum reaction rates, $\varepsilon_{1/2}$ is the spatial distance when λ_c is equal to $\left(\lambda_{\mathrm{c,max}} - \lambda_{\mathrm{c,min}}\right)/2$, h is a Hill coefficient that controls how steep the rate curve is, and ε_{T} is a distance threshold. Eq. [9] can illustrate how the transition rates vary with E-P topologies, and further indicate that transcription is regulated at any time (see more details information in Supplemental Text A). The λ_c can be described using other function based on specific biological issues.

Statistical analysis of the whole model

In the simulation, we examine a system consisting of $N = 100$ monomers in simulations. For a given set of parameters, we simulate 10^3 gene copies, proceeding through 10^7 seconds in time. Each simulation starts in the OFF state. Before taking samples from every simulation, we run 10^4 seconds to ensure equilibration in chromatin conformation and gene expression. After that, snapshots of the system are taken every 100 seconds.

Using the data obtained by simulation, we perform statistical analysis for the chromatin structure,

especially for the E-P spatial distance. Specifically, we calculate the PDF of E-P spatial distance based on the produced time series data. According to the reaction time series, we calculate the probability mass function (PMF) of burst size and the PDFs of the dwell time in S_{OFF} and S_{ON} states and the cycle time (the time from S_{OFF} to S_{ON} and back to S_{OFF}). Furthermore, we calculate some statistical quantities such as mean burst size (MBS), mean dwell-time (MDT) in ON/OFF state, mean cycle time (MCT), burst frequency (BF). Here MBS is defined as the average number of mRNA molecules produced per burst whereas BF as the average number of bursts occurred in a given time interval. In other words, BF is the reciprocal of the MCT.

Theoretical analysis of transcriptional bursting

We deriving the expressions of $p_{BS}(m)$ and $p_{CT}(t)$. For convenience, we uniformly denote these two distributions as $p_X(x)$.

To quantify the timescale separation, we introduce a parameter ω, which is defined as the ratio between the propensities of the reactions on fast and slow timescales

$$\omega = \frac{\min \lambda_{c,\min}}{\max V(\boldsymbol{r})},$$

where $\lambda_{c,\min}$, $c \in \{\text{on1,rec,rel}\}$ are the gene state switching rates in downstream transcription processes and $V(\boldsymbol{r})$ is the velocity field between the enhancer and the promoter in the upstream and is given by $V(\boldsymbol{r}) = (k_{NN}/d_G + k_{EP}) d_S \gamma^{-1}$. The E-P velocity field equals $V(\boldsymbol{r}) = K_{EP} d_S / \gamma$, where K_{EP} represents the total spring coefficient between the enhancer and the promoter. We choose the value of d_S when cumulative density function (CDF) of $p_{DS}(d_S)$ reaches 0.99, implying that the d_S reaches the maximum. Supplemental Figs. S3A-B show the effect of different parameters to ω.

In the case that the fluctuations in d_S are much faster compared with the rate of transcription, the d_S fluctuations can be averaged out, and the corresponding joint distribution denoted by $p^{\text{Fast}}_{X,DS}(x, d_S)$, which accounts for fluctuations in d_S and their effect on fluctuations in burst, is given by $p^{\text{Fast}}_{X,DS}(x, d_S) = p_X(x; \langle \boldsymbol{\lambda} \rangle) p_{DS}(d_S)$, where $\langle \boldsymbol{\lambda} \rangle = \int_0^{+\infty} \boldsymbol{H}(d_S) p_{DS}(d_S) \mathrm{d}d_S$. In this case, the marginal PDF (or PMF) of random variable X takes the form (Supplemental Figs. S3C-D)

$$p^{\text{Fast}}_X(x) = p_{X|\langle DS \rangle}\left(x \middle| \int_0^{+\infty} \boldsymbol{H}(d_S) p_{DS}(d_S) \mathrm{d}d_S \right) \quad [10]$$

On the contrary, if fluctuations in d_S are much slower, the corresponding joint distribution denoted by $p^{\text{Slow}}_{X,DS}(x, d_S)$ is given by $p^{\text{Slow}}_{X,DS}(x, d_S) = p_{X|DS}\left(x \middle| \boldsymbol{H}(d_S)\right) p_{DS}(d_S)$. In this situation, the marginal PDF (or PMF) of random variable X takes the form (Supplemental Figs. S3E-F)

$$p^{\text{Slow}}_X(x) = \int_0^{+\infty} p_{X|DS}\left(x \middle| \boldsymbol{H}(d_S)\right) p_{DS}(d_S) \mathrm{d}d_S \quad [11]$$

In general, the marginal PDF (or PMF) of X is a mixing distribution obtained by weighting the marginal PDF (or PMF). That is

$$p_X(x) = \frac{1}{1+\omega} p^{\text{Fast}}_X(x) + \frac{\omega}{1+\omega} p^{\text{Slow}}_X(x). \quad [12]$$

The expectation of X can be expressed as

$$\langle X \rangle = \frac{1}{1+\omega}\langle X \rangle^{\text{Fast}} + \frac{\omega}{1+\omega}\langle X \rangle^{\text{Slow}}. \quad [13]$$

The detailed derivation process of the E-P spatial distance distribution $p_{DS}(d_S)$ are shown in Supplemental Text B. The downstream transcriptional bursting distribution (ignoring upstream E-P regulatory) can be obtained theoretically (More detailed derivation process in Supplemental Text B).

Power laws for transcriptional bursting kinetics

The power h of Hill function brings difficulties to the theoretical calculations of MBS and MCT. For this reason, we may use a deterministic binary rate for transcriptional burst for approximation and get the approximation expression of MBS_a and MCT_a (Supplemental Text C for more details expression).

In order to show the effects of increasing k_{EP} or d_{G} on MBS and BF, we calculate derivatives: $\partial \log_{10}\text{MBS}/\partial \log_{10} k_{\text{EP}}$ and $\partial \log_{10}\text{BF}/\partial \log_{10} k_{\text{EP}}$, $\partial \log_{10}\text{MBS}/\partial \log_{10} d_{\text{G}}$ and $\partial \log_{10}\text{BF}/\partial \log_{10} d_{\text{G}}$. We take the $\partial \log_{10}\text{MBS}/\partial \log_{10} k_{\text{EP}}$ as an example (the explicit expression is shown in Supplemental Text C).

Through theoretical analysis and numerical calculation, we find $\partial \log_{10}\text{MBS}/\partial \log_{10} k_{\text{EP}}$ are positive when the parameters are not extreme (Supplemental Figs. S5A-C). They increase for small k_{EP} and then quickly decrease to 0 with increasing k_{EP}. Meanwhile, the value of the derivatives changes little (the maximum values are not more than 0.8), implying that linear approximation is appropriate for $\log_{10}\text{MBS}(\log_{10} k_{\text{EP}})$ within an appropriate range of k_{EP}.

Assume that we can obtain $F(k_{\text{EP}_1}) \approx 1$ when k_{EP_1} is greater than a pre-given value, where F is the cumulative distribution of E-P spatial distance distribution, and $\lim_{k_{\text{EP}_2}\to 0} F(k_{\text{EP}_2}) \approx 0.0224$ where $d_{\text{G}} = 50$. We define

$$S_{\text{BS}} = \frac{\log_{10}\text{MBS}(k_{\text{EP}_1}) - \log_{10}\text{MBS}(k_{\text{EP}_2})}{\log_{10} k_{\text{EP}_1} - \log_{10} k_{\text{EP}_2}},$$

which represents the slope of the line of $\log_{10}\text{MBS}$ vs $\log_{10} k_{\text{EP}}$. Then, we obtain the following an approximate linear relation:

$$\begin{aligned}\log_{10}\text{MBS}(k_{\text{EP}}) &\approx S_{\text{BS}} \cdot (\log_{10} k_{\text{EP}} - \log_{10} k_{\text{EP}_1}) + \log_{10}(\text{BS}_{\max}) \\ &= S_{\text{BS}} \cdot \log_{10} k_{\text{EP}} + \log_{10}(\text{BS}_{\max}),\end{aligned}$$

which implies that mean burst size obeys the following power law (Supplemental Fig S6)

$$\text{MBS} \sim (k_{\text{EP}})^{S_{\text{BS}}}. \quad [14]$$

See the Supplemental Text C for the derivation process of other situations.

Software availability

The theoretical analysis and numerical simulation codes are provided as Supplemental Code, and are available online (GitHub: https://github.com/cellfate/4DNucleome).

Competing interest statement

The authors declare no competing interests.

Acknowledgments

This work was supported by National Key R&D Program of China grant 2021YFA1302500; by Natural Science Foundation of P. R. China grants 12171494, 11931019, 11775314, 62373384, 12301646; by Key-Area Research and Development Program of Guangzhou, P.R. China grants 202007030004 and 2019B110233002; by Guangdong Basic and Applied Basic Research Foundation grants 2022A1515011540 and 2023A1515011982; by Guangdong Province Key Laboratory of Computational Science at the Sun Yat-sen University grant 2020B1212060032; by the Fundamental Research Funds for the Central Universities, Sun Yat-sen University grants 23qnpy48 and 23pnqy49; and by the China Postdoctoral Science Foundation grant 2023M734061.

Author contributions: J.Z. conceived of the study. Z.W., Z.Z., S.L. and J.Z. implemented the method, performed the analysis, and interpreted the results. J.Z. supervised the study. Z.W., J.Z. and T.Z. drafted the manuscript with input from all the authors. All authors read and approved the final manuscript.

Reference

Alexander, J.M., Guan, J., Li, B., Maliskova, L., Song, M., Shen, Y., Huang, B., Lomvardas, S., and Weiner, O.D. 2019. Live-cell imaging reveals enhancer-dependent Sox2 transcription in the absence of enhancer proximity. *eLife* **8**: e41769.

Aoi, Y., Smith, E.R., Shah, A.P., Rendleman, E.J., Marshall, S.A., Woodfin, A.R., Chen, F.X., Shiekhattar, R., and Shilatifard, A. 2020. NELF regulates a promoter-proximal step distinct from RNA Pol II pause-release. *Molecular Cell* **78**: 261-274.

Bartman, C.R., Hamagami, N., Keller, C.A., Giardine, B., Hardison, R.C., Blobel, G.A., and Raj, A. 2019. Transcriptional burst initiation and polymerase pause release are key control points of transcriptional regulation. *Molecular Cell* **73**: 519-532.

Bartman, C.R., Hsu, S.C., Hsiung, C.C.-S., Raj, A., and Blobel, G.A. 2016. Enhancer regulation of transcriptional bursting parameters revealed by forced chromatin looping. *Molecular Cell* **62**: 237-247.

Benabdallah, N.S., Williamson, I., Illingworth, R.S., Kane, L., Boyle, S., Sengupta, D., Grimes, G.R., Therizols, P., and Bickmore, W.A. 2019. Decreased enhancer-promoter proximity accompanying enhancer activation. *Molecular Cell* **76**: 473-484.

Bohrer, C.H., and Larson, D.R. 2021. The stochastic genome and its role in gene expression. *Cold Spring Harbor Perspectives in Biology* **13**: a040386.

Bothma, J.P., Garcia, H.G., Ng, S., Perry, M.W., Gregor, T., and Levine, M. 2015. Enhancer additivity and non-additivity are determined by enhancer strength in the Drosophila embryo. *eLife* **4**: e07956.

Braichenko, S., Holehouse, J., and Grima, R. 2021. Distinguishing between models of mammalian gene expression: telegraph-like models versus mechanistic models. *Journal of the Royal Society Interface* **18**: 20210510.

Brivanlou, A.H., and Darnell Jr, J.E. 2002. Signal transduction and the control of gene expression. *Science* **295**: 813-818.

Brouwer, I., and Lenstra, T.L. 2019. Visualizing transcription: Key to understanding gene expression dynamics. *Current Opinion in Chemical Biology* **51**: 122-129.

Brueckner, D.B., Chen, H., Barinov, L., Zoller, B., and Gregor, T. 2023. Stochastic motion and transcriptional dynamics of pairs of distal DNA loci on a compacted chromosome. *Science* **380**: 1357-1362.

Busslinger, G.A., Stocsits, R.R., Van Der Lelij, P., Axelsson, E., Tedeschi, A., Galjart, N., and Peters, J.-M. 2017. Cohesin is positioned in mammalian genomes by transcription, CTCF and Wapl. *Nature* **544**: 503-507.

Cao, Z., Filatova, T., Oyarzún, D.A., and Grima, R. 2020. A stochastic model of gene expression with polymerase recruitment and pause release. *Biophysical Journal* **119**: 1002-1014.

Cattoni, D.I., Gizzi, A.M.C., Georgieva, M., Di Stefano, M., Valeri, A., Chamousset, D., Houbron, C., Déjardin, S., Fiche, J.-B., and González, I. 2017. Single-cell absolute contact probability detection reveals chromosomes are organized by multiple low-frequency yet specific interactions. *Nature communications* **8**: 1753.

Chen, F.X., Xie, P., Collings, C.K., Cao, K., Aoi, Y., Marshall, S.A., Rendleman, E.J., Ugarenko, M., Ozark, P.A., and Zhang, A. 2017. PAF1 regulation of promoter-proximal pause release via enhancer activation. *Science* **357**: 1294-1298.

Chen, H., Levo, M., Barinov, L., Fujioka, M., Jaynes, J.B., and Gregor, T. 2018. Dynamic interplay between enhancer–promoter topology and gene activity. *Nature Genetics* **50**: 1296-1303.

Corrigan, A.M., Tunnacliffe, E., Cannon, D., and Chubb, J.R. 2016. A continuum model of transcriptional bursting. *eLife* **5**: e13051.

Cover, T.M. (1999). Elements of information theory (John Wiley & Sons).

Dekker, J., Belmont, A., Guttman, M., Leshyk, V., Lis, J., Lomvardas, S., Mirny, L., O'Shea, C., Park, P., Ren, B., Politz, J., Shendure, J., Zhong, S., and 4D, N.N. 2017. The 4D nucleome project. *Nature* **549**: 219-226.

Dekker, J., and Mirny, L. 2016. The 3D genome as moderator of chromosomal communication. *Cell* **164**: 1110-1121.

Doi, M., Edwards, S.F., and Edwards, S. (1988). The theory of polymer dynamics (Oxford University Press).

Douglas, A.E. 2018. The Drosophila model for microbiome research. *Lab animal* **47**: 157-164.

Fritzsch, C., Baumgärtner, S., Kuban, M., Steinshorn, D., Reid, G., and Legewie, S. 2018. Estrogen-dependent control and cell-to-cell variability of transcriptional bursting. *Molecular Systems Biology* **14**: e7678.

Fuda, N.J., Ardehali, M.B., and Lis, J.T. 2009. Defining mechanisms that regulate RNA polymerase II transcription in vivo. *Nature* **461**: 186-192.

Fukaya, T., Lim, B., and Levine, M. 2016. Enhancer control of transcriptional bursting. *Cell* **166**: 358-368.

Gardiner, C.W. (2004). Handbook of stochastic methods for physics, chemistry and the natural sciences (Springer).

Gizzi, A.M.C., Cattoni, D.I., Fiche, J.-B., Espinola, S.M., Gurgo, J., Messina, O., Houbron, C., Ogiyama, Y., Papadopoulos, G.L., and Cavalli, G. 2019. Microscopy-based chromosome conformation capture enables simultaneous visualization of genome organization and transcription in intact organisms. *Molecular Cell* **74**: 212-222.

Goutelle, S., Maurin, M., Rougier, F., Barbaut, X., Bourguignon, L., Ducher, M., and Maire, P. 2008. The Hill equation: A review of its capabilities in pharmacological modelling. *Fundamental and Clinical Pharmacology* **22**: 633-648.

Haberle, V., and Stark, A. 2018. Eukaryotic core promoters and the functional basis of transcription initiation. *Nature Reviews Molecular Cell Biology* **19**: 621-637.

Harper, C.V., Finkenstädt, B., Woodcock, D.J., Friedrichsen, S., Semprini, S., Ashall, L., Spiller, D.G., Mullins, J.J., Rand, D.A., and Davis, J.R. 2011. Dynamic analysis of stochastic transcription cycles. *PLoS Biology* **9**: e1000607.

He, B., Chen, C., Teng, L., and Tan, K. 2014. Global view of enhancer–promoter interactome in human cells. *Proceedings of the National Academy of Sciences* **111**: E2191-E2199.

Heinz, S., Texari, L., Hayes, M.G., Urbanowski, M., Chang, M.W., Givarkes, N., Rialdi, A., White, K.M., Albrecht, R.A., and Pache, L. 2018. Transcription elongation can affect genome 3D structure. *Cell* **174**: 1522-1536.

Heist, T., Fukaya, T., and Levine, M. 2019. Large distances separate coregulated genes in living Drosophila embryos. *Proceedings of the National Academy of Sciences* **116**: 15062-15067.

Henriques, T., Scruggs, B.S., Inouye, M.O., Muse, G.W., Williams, L.H., Burkholder, A.B., Lavender, C.A., Fargo, D.C., and Adelman, K. 2018. Widespread transcriptional pausing and elongation control at enhancers. *Genes & Development* **32**: 26-41.

Hübner, M.R., Eckersley-Maslin, M.A., and Spector, D.L. 2013. Chromatin organization and transcriptional regulation. *Current Opinion in Genetics and Development* **23**: 89-95.

Jennings, B.H. 2011. Drosophila–a versatile model in biology & medicine. *Materials Today* **14**: 190-195.

Johnson, D.G., and Walker, C.L. 1999. Cyclins and cell cycle checkpoints. *Annual Review of Pharmacology and Toxicology* **39**: 295-312.

Johnstone, C.P., Wang, N.B., Sevier, S.A., and Galloway, K.E. 2020. Understanding and engineering chromatin as a dynamical system across length and timescales. *Cell Systems* **11**: 424-448.

Jones, D.L., Brewster, R.C., and Phillips, R. 2014. Promoter architecture dictates cell-to-cell variability in gene expression. *Science* **346**: 1533-1536.

Kan, Z., States, D., and Gish, W. 2002. Selecting for functional alternative splices in ESTs. *Genome Research* **12**: 1837-1845.

Kandhavelu, M., Häkkinen, A., Yli-Harja, O., and Ribeiro, A.S. 2012. Single-molecule dynamics of transcription of the

lar promoter. *Physical Biology* **9**: 026004.

Karmakar, R. 2020. Control of noise in gene expression by transcriptional reinitiation. *Journal of Statistical Mechanics: Theory and Experiment* **2020**: 063402.

Karmakar, R., and Das, A.K. 2021. Effect of transcription reinitiation in stochastic gene expression. *Journal of Statistical Mechanics: Theory and Experiment* **2021**: 033502.

Krebs, A.R., Imanci, D., Hoerner, L., Gaidatzis, D., Burger, L., and Schübeler, D. 2017. Genome-wide single-molecule footprinting reveals high RNA polymerase II turnover at paused promoters. *Molecular Cell* **67**: 411-422.

Kumar, N., Platini, T., and Kulkarni, R.V. 2014. Exact distributions for stochastic gene expression models with bursting and feedback. *Physical Review Letters* **113**: 268105.

Lammers, N.C., Kim, Y.J., Zhao, J., and Garcia, H.G. 2020. A matter of time: Using dynamics and theory to uncover mechanisms of transcriptional bursting. *Current Opinion in Cell Biology* **67**: 147-157.

Larson, D.R., Fritzsch, C., Sun, L., Meng, X., Lawrence, D.S., and Singer, R.H. 2013. Direct observation of frequency modulated transcription in single cells using light activation. *eLife* **2**: e00750.

Larsson, A.J.M., Coucoravas, C., Sandberg, R., and Reinius, B. 2019a. X-chromosome upregulation is driven by increased burst frequency. *Nature Structural & Molecular Biology* **26**: 963-969.

Larsson, A.J.M., Johnsson, P., Hagemann-Jensen, M., Hartmanis, L., Faridani, O.R., Reinius, B., Segerstolpe, Å., Rivera, C.M., Ren, B., and Sandberg, R. 2019b. Genomic encoding of transcriptional burst kinetics. *Nature* **565**: 251-254.

Li, J., Hsu, A., Hua, Y., Wang, G., Cheng, L., Ochiai, H., Yamamoto, T., and Pertsinidis, A. 2020. Single-gene imaging links genome topology, promoter–enhancer communication and transcription control. *Nature Structural & Molecular Biology* **27**: 1032-1040.

Li, L., Waymack, R., Gad, M., and Wunderlich, Z. 2021. Two promoters integrate multiple enhancer inputs to drive wild-type knirps expression in the Drosophila melanogaster embryo. *Genetics* **219**: iyab154.

Lim, B., Heist, T., Levine, M., and Fukaya, T. 2018. Visualization of transvection in living Drosophila embryos. *Molecular Cell* **70**: 287-296.

Lim, B., and Levine, M.S. 2021. Enhancer-promoter communication: Hubs or loops? *Current Opinion in Genetics and Development* **67**: 5-9.

Lu, L., Liu, X., Huang, W.-K., Giusti-Rodríguez, P., Cui, J., Zhang, S., Xu, W., Wen, Z., Ma, S., and Rosen, J.D. 2020. Robust Hi-C maps of enhancer-promoter interactions reveal the function of non-coding genome in neural development and diseases. *Molecular Cell* **79**: 521-534. e515.

Marti-Renom, M.A., Almouzni, G., Bickmore, W.A., Bystricky, K., Cavalli, G., Fraser, P., Gasser, S.M., Giorgetti, L., Heard, E., and Nicodemi, M. 2018. Challenges and guidelines toward 4D nucleome data and model standards. *Nature Genetics* **50**: 1352-1358.

Misteli, T. 2020. The self-organizing genome: Principles of genome architecture and function. *Cell* **183**: 28-45.

Murata, M., Gong, P., Suzuki, K., and Koizumi, S. 1999. Differential metal response and regulation of human heavy metal-inducible genes. *Journal of Cellular Physiology* **180**: 105-113.

Neuert, G., Munsky, B., Rui, Z.T., Teytelman, L., Khammash, M., and Oudenaarden, A.V. 2013. Systematic identification of signal-activated stochastic gene regulation. *Science* **339**: 584-587.

Ochiai, H., Hayashi, T., Umeda, M., Yoshimura, M., Harada, A., Shimizu, Y., Nakano, K., Saitoh, N., Liu, Z., and Yamamoto, T. 2020. Genome-wide kinetic properties of transcriptional bursting in mouse embryonic stem cells. *Science Advances* **6**: eaaz6699.

Ou, H.D., Phan, S., Deerinck, T.J., Thor, A., Ellisman, M.H., and O'shea, C.C. 2017. ChromEMT: Visualizing 3D chromatin structure and compaction in interphase and mitotic cells. *Science* **357**: eaag0025.

Perry, M.W., Boettiger, A.N., Bothma, J.P., and Levine, M. 2010. Shadow enhancers foster robustness of Drosophila gastrulation. *Current Biology* **20**: 1562-1567.

Pott, S., and Lieb, J.D. 2015. What are super-enhancers? *Nature Genetics* **47**: 8-12.

Robson, M.I., Ringel, A.R., and Mundlos, S. 2019. Regulatory landscaping: How enhancer-promoter communication is sculpted in 3D. *Molecular Cell* **74**: 1110-1122.

Rodriguez, J., and Larson, D.R. 2020. Transcription in living cells: Molecular mechanisms of bursting. *Annual Review of Biochemistry* **89**: 189-212.

Rodriguez, J., Ren, G., Day, C.R., Zhao, K., Chow, C.C., and Larson, D.R. 2019. Intrinsic dynamics of a human gene reveal the basis of expression heterogeneity. *Cell* **176**: 213-226.

Senecal, A., Munsky, B., Proux, F., Ly, N., Braye, F.E., Zimmer, C., Mueller, F., and Darzacq, X. 2014. Transcription factors modulate c-Fos transcriptional bursts. *Cell Reports* **8**: 75-83.

Shahrezaei, V., and Swain, P.S. 2008. Analytical distributions for stochastic gene expression. *Proceedings of the National Academy of Sciences* **105**: 17256-17261.

Shannon, C.E. 1948. A mathematical theory of communication. *The Bell system technical journal* **27**: 379-423.

Shao, W., and Zeitlinger, J. 2017. Paused RNA polymerase II inhibits new transcriptional initiation. *Nature Genetics* **49**: 1045-1051.

Sood, V., and Misteli, T. 2022. The stochastic nature of genome organization and function. *Current Opinion in Genetics and Development* **72**: 45-52.

Stadhouders, R., Filion, G.J., and Graf, T. 2019. Transcription factors and 3D genome conformation in cell-fate decisions. *Nature* **569**: 345-354.

Stavreva, D.A., Coulon, A., Baek, S., Sung, M.H., John, S., Stixova, L., Tesikova, M., Hakim, O., Miranda, T., and Hawkins, M. 2015. Dynamics of chromatin accessibility and long-range interactions in response to glucocorticoid pulsing. *Genome Research* **25**: 845-857.

Su, J.-H., Zheng, P., Kinrot, S.S., Bintu, B., and Zhuang, X. 2020. Genome-scale imaging of the 3D organization and transcriptional activity of chromatin. *Cell* **182**: 1641-1659.

Suter, D.M., Molina, N., Gatfield, D., Schneider, K., Schibler, U., and Naef, F. 2011. Mammalian genes are transcribed with widely different bursting kinetics. *Science* **332**: 472-474.

Sutherland, H.G., Martin, D.I., and Whitelaw, E. 1997. A globin enhancer acts by increasing the proportion of erythrocytes expressing a linked transgene. *Molecular and Cellular Biology* **17**: 1607-1614.

Szavits-Nossan, J., and Grima, R. 2023. Steady-state distributions of nascent RNA for general initiation mechanisms. *Physical Review Research* **5**: 013064.

Thomas, P., Popović, N., and Grima, R. 2014. Phenotypic switching in gene regulatory networks. *Proceedings of the National Academy of Sciences* **111**: 6994-6999.

Tunnacliffe, E., and Chubb, J.R. 2020. What is a transcriptional burst? *Trends in Genetics* **36**: 288-297.

Walters, M.C., Fiering, S., Eidemiller, J., Magis, W., Groudine, M., and Martin, D. 1995. Enhancers increase the probability but not the level of gene expression. *Proceedings of the National Academy of Sciences* **92**: 7125-7129.

Wang, Z., Zhang, Z., and Zhou, T. 2020. Exact distributions for stochastic models of gene expression with arbitrary regulation. *Science China Mathematics* **63**: 485-500.

Weidemann, D.E., Holehouse, J., Singh, A., Grima, R., and Hauf, S. 2023. The minimal intrinsic stochasticity of constitutively expressed eukaryotic genes is sub-Poissonian. *Science Advances* **9**: eadh5138.

Xiao, J.Y., Hafner, A., and Boettiger, A.N. 2021. How subtle changes in 3D structure can create large changes in transcription. *eLife* **10**: e64320.

Yokoshi, M., Segawa, K., and Fukaya, T. 2020. Visualizing the role of boundary elements in enhancer-promoter communication. *Molecular Cell* **78**: 224-235.

Zabidi, M.A., and Stark, A. 2016. Regulatory enhancer–core-promoter communication via transcription factors and cofactors. *Trends in Genetics* **32**: 801-814.

Zhang, J., and Zhou, T. 2014. Promoter-mediated transcriptional dynamics. *Biophysical Journal* **106**: 479-488.

Zhang, J., and Zhou, T. 2019. Markovian approaches to modeling intracellular reaction processes with molecular memory. *Proceedings of the National Academy of Sciences* **116**: 23542-23550.

Zuin, J., Roth, G., Zhan, Y., Cramard, J., Redolfi, J., Piskadlo, E., Mach, P., Kryzhanovska, M., Tihanyi, G., and Kohler, H. 2022. Nonlinear control of transcription through enhancer-promoter interactions. *Nature* **604**: 571-577.

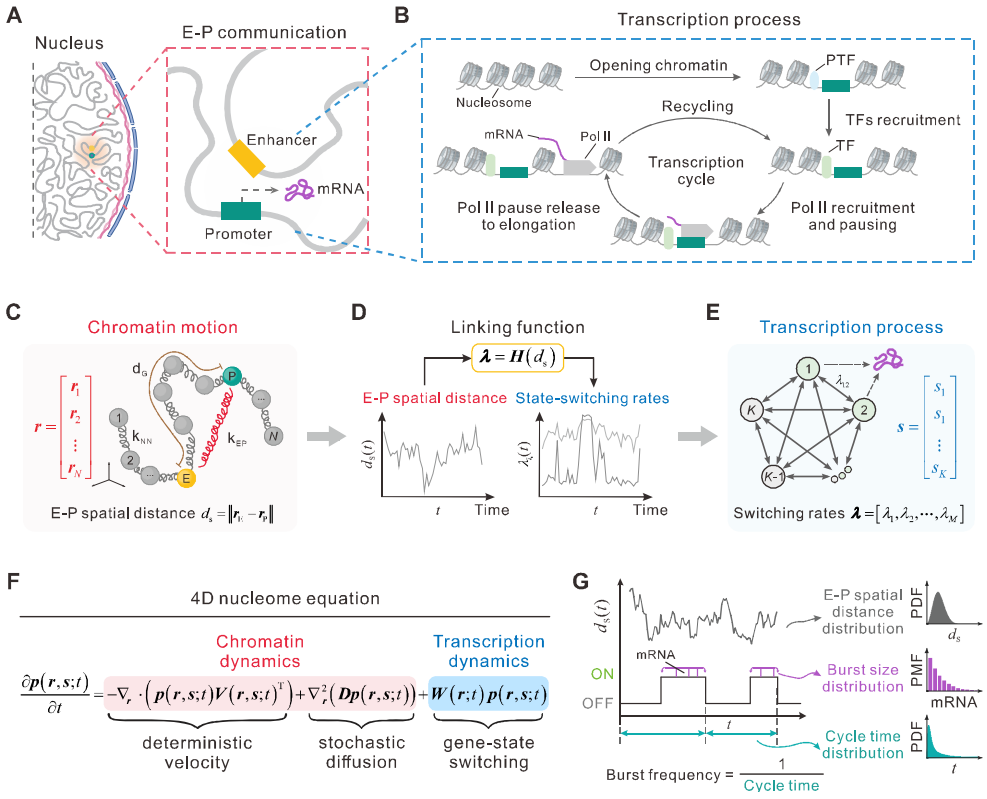

Figure 1. A framework for modeling how E-P communication regulates transcription dynamics. (**A**, **B**) Schematic for a biological model: The upstream E-P communication in cell nucleus (**A**) guides the downstream transcription, which is a multistep process where only the main steps are depicted (**B**). (**C**, **D**, **E**) Schematic for a physical model: A generalized Rouse model is proposed to model chromatin spatial motion including E-P communication (indicated by the red spring with coefficient k_{EP}), where $\boldsymbol{r} = [\boldsymbol{r}_1, \cdots, \boldsymbol{r}_N]^{\mathrm{T}}$ represents nucleosome positions in 3D (**C**); A link function vector $\boldsymbol{\lambda} = \boldsymbol{H}(d_{\mathrm{s}})$ bridges the temporal disconnection between the upstream and the downstream (**D**), where d_{s} is the E-P spatial distance and $\boldsymbol{H}$ is a Hill-like function vector; And (**E**) schematically shows a transcription process, where $\boldsymbol{s} = [s_1, \cdots, s_K]^{\mathrm{T}}$ is the vector of the gene's states, and $\boldsymbol{\lambda}$ is a vector of state switching rates. (**F**, **G**) Mathematical model: A 4D nucleome equation (**F**) is derived to model the spatiotemporal evolution of the entire system, and the characteristics of the three distributions of interest are schematically demonstrated (**G**).

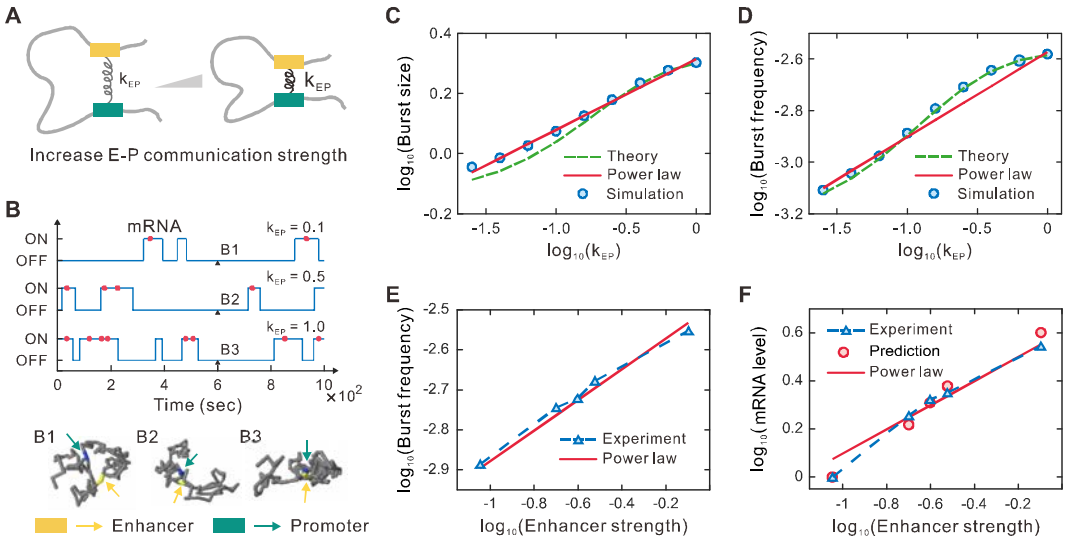

Figure 2. Effect of the E-P communication strength on transcriptional bursting kinetics. (**A**) Schematic illustration of the augment of E-P communication strength k_{EP}. (**B**) Example traces of binarized transcriptional activity for three different values of k_{EP}, where red points represent the mRNA generation events and the corresponding 3D chromatin structures are shown on the bottom. (**C**) Log-log plot for the relationship between mean burst size and strength k_{EP}. The green dashed line represents the theoretical result, whereas blue circles show numerical simulations. The red solid line indicates a power-law approximation (Eq. [3]) with a scaling exponent $S_{\mathrm{BS}} = 0.23$. (**D**) Log-log plot for the relationship between burst frequency and k_{EP}. Meanings of symbols are the same as those in (**C**), but the scaling exponent is $S_{\mathrm{BF}} = 0.33$. (**E-F**) Log-log plot of experimental data from (Fukaya et al., 2016). The x-axis shows the E-P communication strengths of different enhancers, obtained by theoretical inferring based on the burst frequency data (converted the unit into sec^{-1}). The red points in (**F**) represent the theoretical result of mRNA level (converting its trend of change into a fold change) while the blue dashed line shows the experimental data (Fluorescence intensity is a relative value, converting its trend of change into a fold change).

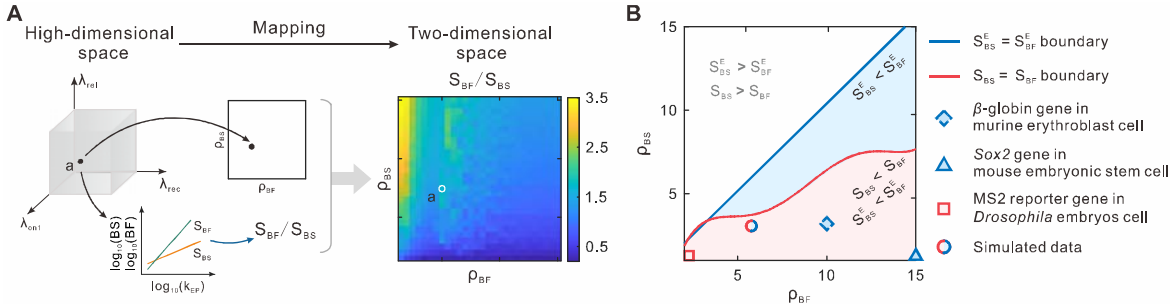

Figure 3. Separatrixes for power-law behaviors of BS and BF in the (ρ_{BF},ρ_{BS}) plane. (**A**) Schematic illustration of the dimension reduction method, where a high-dimensional parameter space is mapped into the (ρ_{BF},ρ_{BS}) space and the calculated values of S_{BF}/S_{BS} (the bottom inset) are plotted in the (ρ_{BF},ρ_{BS}) plane (the heatmap). (**B**) The red line stands for the boundary obtained by smoothing the theoretical results S_{BF}/S_{BS}, the blue line for the boundary obtained by smoothing the theoretical results S^E_{BF}/S^E_{BS} (after enhancer deletion). The colored regions indicate that E-P communication affects BF more than BS under different situations. The square at point $(2.3,1.3)$ corresponds to the MS2 reporter gene in *Drosophila* embryos cell in (Fukaya et al., 2016), the triangle at point $(15,1.4)$ to the *Sox2* gene in mouse embryonic stem cell in (Larsson et al., 2019b), the dashed diamond at point $(\cdot,3.3)$ to the *β*-globin gene in murine erythroblast cell in (Bartman et al., 2016), and the red blue mixed circle to the simulated data. Note that the burst frequency in (Larsson et al., 2019b) defined as the reciprocal of OFF state dwell-time, which is approximately converted to the reciprocal of cycle time, and that the ρ_{BF} at the dashed diamond point $(\cdot,3.3)$ related to burst fraction in (Bartman et al., 2016) is approximate. By the blue region, we mean the whole area below the blue line (some part is covered by red regions).

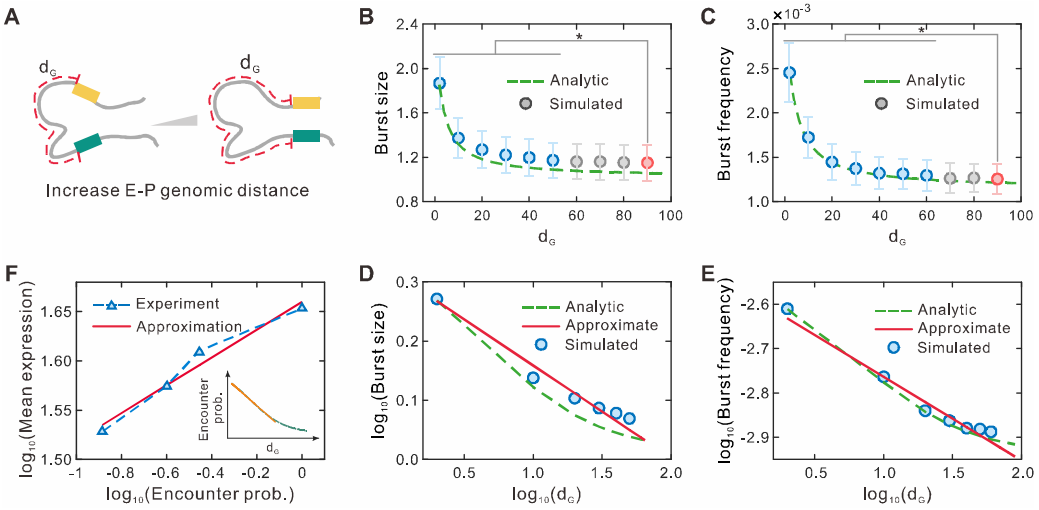

Figure 4. Effect of E-P genomic distance on transcriptional bursting kinetics. (**A**) A schematic diagram shows the increment of E-P genomic distance d_G. (**B**) Influence of d_G on burst size. Dashed green line represents the theoretical result whereas circles show numerical simulations. The blue circles indicate significant differences compared to the end data point (red) via Kruskal-Wallis nonparametric test, while the gray circles indicate no significance. (**C**) Influence of d_G on burst frequency, where the meanings of all symbols are the same as those in (**B**). (**D**) Log-log plot shows the relationship between mean burst size and d_G. Blue circles are the data points with significant differences in (**B**). The red solid line indicates the power-law approximation (Eq. [4]) with the scaling exponent $\ell_{BS} = -0.16$. Meanings of the symbols are also similar to those in (**B**). (**E**) Log-log plot shows the relationship between burst frequency and d_G. Meanings of the symbols are similar to those in (**D**) but the scaling exponent is $\ell_{BF} = -0.19$. (**F**) Log-log plot of experimental data from (Zuin et al., 2022). Insert figure shows the log-log relationship between d_G and encounter probability. The yellow line indicates an approximate power-law relationship for smaller d_G.

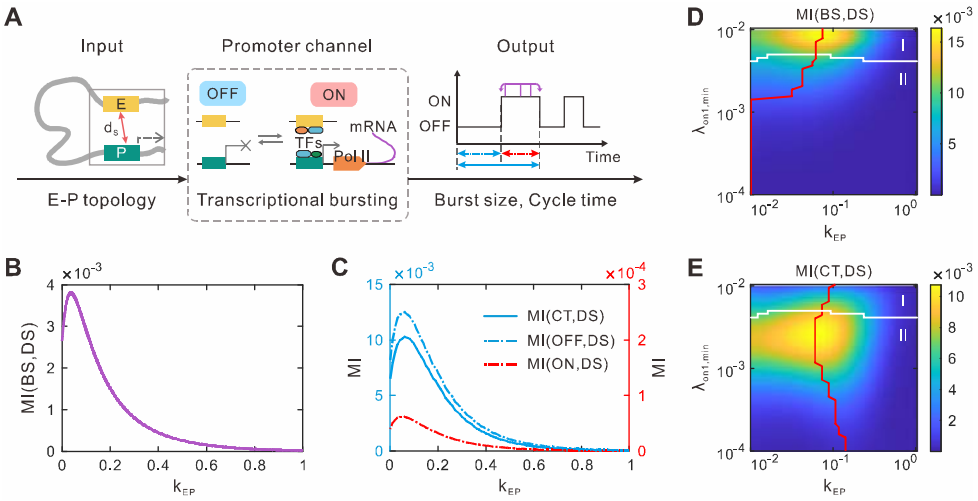

Figure 5. Mutual information reveals the effect of E-P communication on bursting kinetics. (**A**) An information theoretic framework is used to study the effect of input E-P topology on bursting output. The promoter governing transcriptional bursting can be considered a noisy channel. (**B**) Mutual information between E-P spatial distance and burst size ($\mathrm{MI}(BS,DS)$) as a function of E-P communication strength k_{EP}. (**C**) Mutual information between E-P spatial distance and cycle time (or OFF time, ON time) as a function of k_{EP}. (**D-E**) Heatmap shows the effect of k_{EP} and minimum rate $\lambda_{\mathrm{on1,min}}$ on $\mathrm{MI}(BS,DS)$ (**D**) and on $\mathrm{MI}(CT,DS)$ (**E**). The red line shows the values of k_{EP} obtained from the MMIs with different $\lambda_{\mathrm{on1,min}}$. The white line is the separatrix between the values of $\mathrm{MI}(BS,DS)$ and $\mathrm{MI}(CT,DS)$. Region I stands for $\mathrm{MI}(DS,BS) > \mathrm{MI}(DS,CT)$ whereas region II for $\mathrm{MI}(DS,BS) < \mathrm{MI}(DS,CT)$.